

# Low-Temperature Water–Gas Shift: Doping Ceria Improves Reducibility and Mobility of O-Bound Species and Catalyst Activity

Linda Z. Linganiso · Venkat Ramana Rao Pendyala · Gary Jacobs · Burtron H. Davis · Donald C. Cronauer · A. Jeremy Kropf · Christopher L. Marshall

Received: 18 August 2011 / Accepted: 3 October 2011 / Published online: 25 October 2011  
© Springer Science+Business Media, LLC 2011

**Abstract** A series of platinum loaded catalysts supported on cation (Me)-doped cerium dioxide (Me = Ba, La, Y, Hf and Zn) was prepared by co-precipitation of the Me-nitrates and impregnation of a Pt precursor. Low temperature water–gas shift activity depends on the nature of dopant employed, varying in the order of Ba > Y > Hf > La > undoped ceria > Zn. TPR-XANES measurements with flowing hydrogen reveal that adding dopants to ceria facilitate ceria reduction and increases the extents of both surface shell and bulk reduction of ceria. Experimental results confirm past theoretical models that dopants enhance both O-mobility and reducibility of ceria. DRIFTS measurements of the transient decomposition of formates in steam suggest that formate half-life follows the trend Zn > undoped ceria > La > Hf > Y > Ba, indicating that the formate decomposition rate is enhanced by the addition of most of the dopants tested. Taken together, the results suggest that dopant addition improves the WGS rate by increasing the O-mobility of O-bound associated intermediates. Therefore, less Pt and Ce, which are expensive, is required to achieve comparable levels of activity.

**Keywords** Water–gas shift · Cerium oxide · Platinum · Doping · TPR-XANES

## 1 Introduction

The water–gas shift reaction (WGS) plays a critical role in the production of hydrogen from fossil and renewable resources. It has attracted great attention because of its applications in producing syngas for chemicals and liquid fuels, providing hydrogen-rich streams for fuel cells [1, 2] and processing exhaust gases from automobiles [3–6]. WGS is a reversible and an exothermic chemical reaction and thus limited by thermodynamic equilibrium at high temperatures. At low temperatures, the thermodynamics are favorable, but the reaction is constrained by slow kinetics. Commercially, the WGS reaction is performed in two stages to overcome the thermodynamic and kinetic limitations of the reaction. The two steps involve a high-temperature (350–500°C) shift (HT-WGS) reaction typically over Fe<sub>2</sub>O<sub>3</sub>/Cr<sub>2</sub>O<sub>3</sub> catalysts at which thermodynamics limits the equilibrium conversion [1], followed by a low temperature (200–250°C) shift (LT-WGS) reaction over a Cu/ZnO-based catalysts, in which thermodynamics are favorable but the reaction rate is constrained by kinetics, such that highly active catalysts are necessary to provide adequate activity.

Precious metals dispersed on partially reducible oxides (PRO) e.g., ceria, zirconia, thoria, and titania are reported as promising catalysts for LTS in fuel processors for fuel cell applications, because they exhibit high activity and are non-pyrophoric relative to the conventional Cu/ZnO/Al<sub>2</sub>O<sub>3</sub> catalyst, an important factor considering that the catalyst should be resistant to repeated start-up/shut-down cycles [7, 8]. The WGS activity of ceria-supported precious metal catalysts can be enhanced significantly by addition of surface promoters [9–14]. This has been attributed to the effects induced by the presence of promoters on the surface properties of ceria [14], including reducibility, oxygen

---

L. Z. Linganiso · V. R. R. Pendyala · G. Jacobs · B. H. Davis (✉)  
University of Kentucky Center for Applied Energy Research,  
2540 Research Park Drive, Lexington, KY 40511, USA  
e-mail: burtron.davis@uky.edu

D. C. Cronauer · A. J. Kropf · C. L. Marshall  
Chemical Sciences and Engineering Division, Argonne National  
Laboratory, 9700 South Cass Avenue, CSE/205, Argonne  
IL 60439-4837, USA

storage capacity and resistance to sintering [13]. It has been also proposed that the role of the promoter is to lower the barrier for oxygen transfer from ceria to the metal [9], thereby facilitating oxidation of adsorbed CO. Recently we have conducted numerous studies with Pt/CeO<sub>2</sub> catalysts, and our findings support a low-temperature WGS reaction mechanism involving surface formate intermediates, as proposed by Shido and Iwasawa [15, 16]. The catalytically active sites for formation of the intermediate were found to be Type II bridging OH groups [15–19] on partially reduced ceria, and these react with CO to generate surface formates. The relative stability of the formates at low temperature is such that their decomposition is proposed to be the elementary step that is rate limiting. However, another important consideration is that mounting evidence suggests that H<sub>2</sub>O promotes the forward decomposition rate of surface formates during WGS to H<sub>2</sub> and unidentate carbonate [15, 16], which decomposes to CO<sub>2</sub> to regenerate the OH groups, completing the catalytic cycle. We have recently verified the autocatalytic role of H<sub>2</sub>O in transient formate decomposition experiments [20]. One role of the metal (e.g., Pt, Rh) is to promote the surface reduction of ceria to generate the active bridging OH groups at lower temperatures [15, 21].

The activity of fresh Pt/ceria catalysts was found to be not enough to meet the weight and cost constraints found in automotive applications [22]. As a result, efforts are made to further increase catalytic activity and to improve structural stability of ceria-supported noble metal catalysts. Current research aims to reduce costs by restricting the amounts of both precious and rare earth metals involved in the catalyst formulation. It was demonstrated [23] that both higher formate decomposition and low-temperature shift rates are achieved at a significant cost if one resorts to increasing Pt levels. Thus, another role of Pt is to assist in promoting formate decomposition by assisting in H-abstraction, where Pt is a porthole for H<sub>2</sub> removal [23]. Increasing Pt loading improves the reducibility of the catalyst, thus increasing the number of active bridging OH groups on the surface, and increases the platinum-ceria interface to increase the formate turnover rate. However, the problem of decreasing noble metal loadings while maintaining high activity poses a significant challenge. Less surface intermediate in the rapid reaction zone (RRZ) [24] close to the platinum-ceria interface means that, if the amount of Pt is to be decreased, either (a) the dispersion of Pt must be increased or (b) the rate of surface diffusion of associated intermediates to the platinum-ceria interface must be enhanced. In the first case, one challenge is that the metal-support interaction [23, 25] prevents activation of the catalyst components (i.e., reduction of Pt and the ceria surface shell) within temperatures needed for LTS. In the latter case, there is no guarantee of improved CO

conversion rates if decomposition of the surface intermediate is slow relative to its surface diffusion rate. As explained by Duprez [26], oxygen mobility in the partially reducible oxide (PRO) may be an important parameter that could be developed to improve the surface diffusion rates of O-bound intermediates during low-temperature water-gas shift, such that reaction intermediates (e.g., formates and carbonates [8, 23] or perhaps carboxylates [27]) are supplied at adequate rates to the platinum-ceria interface. Although carboxylates have recently been suggested as alternative surface intermediates to formates/carbonates, it should be noted that the species has not been identified by infrared spectroscopy, which is not a satisfying conclusion. Our view on this subject and continued support of the formate mechanism is described in a recent research account [28].

Metal-modified ceria has higher oxygen storage capacity and enhanced reducibility than pure ceria. The addition of metal dopants leads to the formation of oxygen vacancies in ceria, which is expected to increase the redox activity [29]. The addition of dopants to ceria may have two consequences: (1) to increase the number of oxygen vacancies in the ceria structure and (2) to improve the reducibility by weakening the Ce–O bond through lattice strain. In the present study we performed a comparative analysis regarding these aspects using as examples platinum catalysts supported on ceria doped by Ba, La, Y, Hf and Zn. The nature of the dopants and their influence on catalyst reducibility, formate mobility, and WGS activity, are discussed. Special emphasis is placed on using time resolved EXAFS and XANES, a technique that has been successfully applied for examining the oxygen storage and release properties of CeO<sub>2</sub>–ZrO<sub>2</sub> mixed oxides [30].

## 2 Experimental

### 2.1 Catalyst Preparation

High surface area mixed oxide solid solutions of Ce<sub>x</sub>Me<sub>1–x</sub>O<sub>y</sub> were prepared via a homogenous precipitation of cerium and nitrate salt of the dopant, using NaOH (Sigma-Aldrich, 97%, 20–40 mesh beads) as the precipitating agent. In this method, appropriate amounts of Ce(NO<sub>3</sub>)<sub>3</sub>·6H<sub>2</sub>O (Alfa Aesar, 99.5%) and nitrate salt of the dopant were first dissolved simultaneously in deionized water at room temperature. The total metal ion concentration was maintained at 1 M for all experiments. The nitrate salt of dopants was stirred at 500 RPM at room temperature until completely dissolved. The nitrate salt of dopant solution was slowly added drop-wise to a sodium hydroxide solution (1 M), accompanied by constant stirring at 700 RPM to avoid the formation of lumps and to

ensure a complete dissolution. The pH was maintained at  $\sim 12$  to ensure simultaneous precipitation of dopants and ceria. The solution was refluxed at  $80^\circ\text{C}$  with constant stirring (500 RPM) for 20 h. The resulting precipitate was filtered and suspended in 4 L of deionized water a total of three times, and each time the solution was stirred for 1 h at room temperature to remove Na ions. The resulting residue was filtered and washed thoroughly with deionized water. It was then dried in a static oven at  $110^\circ\text{C}$  overnight. The solid material obtained was crushed and the resulting powder was calcined in air in a muffle furnace at  $400^\circ\text{C}$  for 4 h.

To the resulting supports, platinum was deposited via incipient wetness impregnation by taking into consideration the pore volume of the support as measured by  $\text{N}_2$  physisorption. Appropriate amounts of  $\text{Pt}(\text{NH}_3)_4(\text{NO}_3)_2$  (Alfa Aesar, 99%) were dissolved in deionized water, and the solution was added drop-wise to the supports to obtain 0.5% by weight Pt. The resulting material was dried in a static oven overnight at  $110^\circ\text{C}$  and then calcined at  $400^\circ\text{C}$  for 4 h. Before testing, the catalyst samples were pelletized at 15 tons per square inch for 5 s and sieved in the diameter range of  $355\ \mu\text{m} < \Phi < 600\ \mu\text{m}$ .

## 2.2 BET Surface Area and Porosity

BET surface area was determined using a Micromeritics TRISTAR 3000 gas adsorption analyzer. In each test, approximately 0.30 g of the sample was used. The adsorption gas was nitrogen and the sample analyses were performed at the boiling temperature of liquid nitrogen. Samples were degassed under vacuum for 12 h before conducting the nitrogen adsorption measurements. The specific surface areas were determined by the Brunauer–Emmett–Teller (BET) method.

## 2.3 X-ray Absorption Near Edge Spectroscopy (XANES)

In situ  $\text{H}_2$ -TPR XAFS studies were performed at the Materials Research Collaborative Access Team (MR-CAT) beamline at the Advanced Photon Source, Argonne National Laboratory. A cryogenically cooled Si (111) monochromator selected the incident energy and a rhodium-coated mirror rejected higher order harmonics of the fundamental beam energy. The experiment setup was similar to that outlined by Jacoby [31]. A stainless steel multi-sample holder (4.0 mm i.d. channels) was used to monitor the in situ reduction of six samples during a single TPR run. The catalyst samples were diluted with silica gel at a weight ratio (silica/sample) of approximately 4.0. Approximately 3.0 mg of each sample was loaded as a self-supporting wafer in each channel. The holder was placed in

the center of a quartz tube, equipped with gas and thermocouple ports and Kapton windows. The amount of sample used was optimized for the Ce  $L_{\text{III}}$  edge (5723 eV). The quartz tube was placed in a clamshell furnace mounted on a positioning table. Each sample cell was positioned relative to the beam by finely adjusting the position of the table to an accuracy of  $20\ \mu\text{m}$  (for repeated scans). Once the sample positions were fine-tuned, the reactor was purged with helium for more than 5 min at 30 ml/min. Then, the reactant gas ( $\text{H}_2/\text{He}$ , 4%) was flowed through the samples (30 ml/min) and a temperature ramp of  $\sim 1.8^\circ\text{C}/\text{min}$  was initiated for the furnace. Samples were ramped to  $\sim 980^\circ\text{C}$ .

The Ce  $L_{\text{III}}$ -edge spectra were recorded in transmission mode and a Cr metallic foil spectrum was measured simultaneously with each sample spectrum for energy calibration. X-ray absorption spectra for each sample were collected from 5623 to 6032 eV, with a step size of 0.40 eV and acquisition times of 30 s per spectrum. By measuring each sample, in turn, and repeating, this allowed 182 scans to be collected for each sample over a 7.5 h period. A sample's temperature change from the absorption edge through the end of the scan was then about  $0.7^\circ\text{C}$ , while a spectrum was measured approximately every  $0.9^\circ\text{C}$ . Data reduction of the XAFS spectra was carried out using the WinXAS program [32], and raw data were processed to give the normalized XANES spectra. Linear combination fitting of spectra with appropriate reference compounds was carried out. The initial spectrum of each catalyst was used as a fingerprint for the  $\text{Ce}^{4+}$  oxidation state, while the final spectrum of the 0.5%Pt/Hf<sub>0.50</sub>Ce<sub>0.50</sub>O<sub>x</sub> catalyst following TPR was used as a fingerprint of the  $\text{Ce}^{3+}$  oxidation state for all samples, since its lineshape resembled  $\text{Ce}^{3+}$  compounds, such as  $\text{Ce}(\text{NO}_3)_3$ .

## 2.4 Diffuse Reflectance Fourier Transform Infrared Spectroscopy (DRIFTS)

A Nicolet Nexus 870 infrared spectrometer was used equipped with a DTGS-TEC detector. A chamber fitted with ZnSe windows was utilized as the WGS reactor for in situ measurements. Experimental procedures are provided elsewhere [33]. For each run, the catalyst was first activated at  $350^\circ\text{C}$  in 50 ml/min of 33%  $\text{H}_2$  (balance He) for 2 h and then cooled to  $130^\circ\text{C}$ . Formates were generated using the following procedure. Steady state low-temperature shift was first carried out at  $225^\circ\text{C}$  using a mixture consisting of 37.5 ml/min of 10% CO/He, 62.5 ml/min of  $\text{H}_2\text{O}$ , and 33.75 ml/min He. This condition produces a rate-limited coverage of surface formate on the catalyst surface. To achieve a high coverage of formate,  $\text{H}_2\text{O}$  was switched off and CO adsorption was carried out using 37.5 ml/min of 10% CO/He and 96.25 ml/min He. When  $\text{H}_2\text{O}$  is

completely removed from the system, formate generated from reaction of Type II bridging OH groups and CO cannot at low temperature undergo forward decomposition to hydrogen and unidentate carbonate, the latter being the precursor to CO<sub>2</sub> formation. Thus, when the water is switched off, the steady state formate coverage increases. After the formate was generated, the temperature was lowered to 130°C and the catalyst was then exposed to H<sub>2</sub>O vapor generated from a bubbler using helium at 50 ml/min. Since decomposition of formate was found to be quite rapid in previous transient formate decomposition studies [20, 34, 35] when the concentration of H<sub>2</sub>O was high (e.g., 32–56%), which is typical of steady state fuel processor conditions, the decision was made to significantly slow down the forward formate decomposition rate by employing only 3% H<sub>2</sub>O as produced using the bubbler. It should be noted that, after a complete coverage of formate is generated on the surface of Pt/ceria, when exposed to H<sub>2</sub>O the formates have been observed to decompose completely in the LTS temperature range in ~20 s [36]. During decomposition, an intense CO<sub>2</sub> peak was observed due to forward decomposition, which stopped only after no formate remained on the surface.

## 2.5 Catalytic Testing Using a Fixed Bed Reactor

Catalytic tests for the LT-WGS reaction were carried out in a stainless steel fixed-bed tubular reactor (0.444 in i.d.) under steady state conditions. Typically, the catalysts were pressed into pellets, crushed, and sieved to yield grains of 355–600 μm in diameter. A 200-mg catalyst sample diluted with 1800-mg glass beads (60–80 μm in size) was packed between two layers of quartz wool. Using the glass beads ensured plug flow was maintained and minimized the effect of heat generated by the mildly exothermic reaction. The temperature of the catalyst bed was monitored by a thermocouple (Fe–Cr) and maintained by a temperature controller (Ω Omega CN 3251-R). Prior to testing, the catalysts were first reduced in H<sub>2</sub> (100 ml/min) at 350°C for 1 h (ramp of 4°C/min). A gas mixture containing 3.0% CO, 26.1% H<sub>2</sub>O, 29.9% H<sub>2</sub>, 3.7% N<sub>2</sub> (balance He) was used for the catalytic tests to mimic, except for the case of CO<sub>2</sub>, LTS conditions found in a typical fuel processor for fuel cell applications. The dry gases were controlled using Brooks mass flow controllers. Steam was provided to the system via a steam generator consisting of a hollow cylinder (50 mm i.d., 150 mm long) packed with quartz wool. Water was fed by infusion with a syringe pump (Thermo scientific, model Orion M361) into the steam generator via a 1/16 in. needle with a side-port hole. The whole system was heated to 180°C to avoid condensation of H<sub>2</sub>O. The feed was adjusted in bypass mode to obtain a steady state concentration of CO/H<sub>2</sub>O/N<sub>2</sub>/H<sub>2</sub>/He prior to

bringing the catalyst online (concentration = 3.0/26.1/3.7/29.9/37.3 mol%, where N<sub>2</sub> was used as an internal standard). The products were passed through a cold trap cooled to 0°C to condense water from the gas prior to GC analysis. The SRI 8610C GC includes two columns [6 ft (3.658 m) silica gel packed and 3 ft (1.829 m) molecular sieve packed] and two detectors (FID and TCD). To boost the sensitivity of the CO and CO<sub>2</sub> signals, the GC incorporates a methanizer, such that these products can be analyzed by FID.

## 3 Results and Discussion

### 3.1 BET Surface Area and Porosity

The results of nitrogen physisorption obtained for support materials are summarized in Table 1, and the corresponding 0.5% platinum loaded catalysts are shown in Table 2. The BET surface area of the as prepared pure ceria was found to be 114 m<sup>2</sup>/g. Doped ceria support surface areas were found to be higher or lower than pure ceria, and may depend on the surface area of the dopant. After the platinum impregnation, the surface areas dropped somewhat more than if the ceria or doped ceria were the only contributor to the area. This decrease in the BET surface area upon platinum impregnation is attributed to a fraction of

**Table 1** BET surface area and porosity measurements from nitrogen physisorption at 77K for support materials

Catalyst	BET surface area (m <sup>2</sup> /g)	Pore volume (cm <sup>3</sup> /g)	Average pore radius (nm)
CeO <sub>2</sub>	114.1	0.4	6.6
Ce <sub>0.5</sub> Ba <sub>0.5</sub> O <sub>1.5</sub>	65.63	0.36	10.2
Ce <sub>0.5</sub> Hf <sub>0.5</sub> O <sub>2</sub>	172.98	0.24	2.6
Ce <sub>0.5</sub> La <sub>0.5</sub> O <sub>1.75</sub>	89.63	0.54	10.5
Ce <sub>0.5</sub> Y <sub>0.5</sub> O <sub>1.75</sub>	61.1	0.35	10.5
Ce <sub>0.5</sub> Zn <sub>0.5</sub> O <sub>1.5</sub>	134.65	0.29	3.7

**Table 2** BET surface area and porosity measurements from nitrogen physisorption at 77K for 0.5% platinum loaded support materials

Catalyst	BET surface area (m <sup>2</sup> /g)	Pore volume (cm <sup>3</sup> /g)	Average pore radius (nm)
0.5%Pt/CeO <sub>2</sub>	112.9	0.33	6.3
0.5%Pt/Ce <sub>0.5</sub> Ba <sub>0.5</sub> O <sub>1.5</sub>	56.6	0.27	9.22
0.5%Pt/Ce <sub>0.5</sub> Hf <sub>0.5</sub> O <sub>1.5</sub>	167.87	0.24	2.61
0.5%Pt/Ce <sub>0.5</sub> La <sub>0.5</sub> O <sub>1.5</sub>	89.87	0.56	10.76
0.5%Pt/Ce <sub>0.5</sub> Y <sub>0.5</sub> O <sub>1.5</sub>	60.8	0.35	10.83
0.5%Pt/Ce <sub>0.5</sub> Zn <sub>0.5</sub> O <sub>1.5</sub>	128.52	0.27	3.63

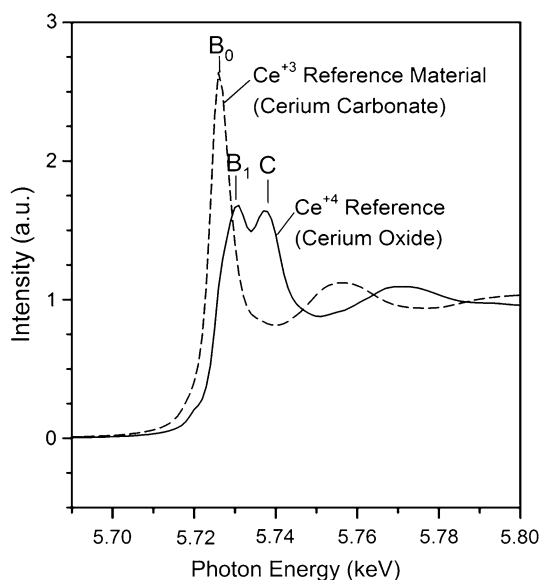


**Fig. 1** XANES spectra of reference compounds for  $\text{Ce}^{3+}$  (cerium carbonate) and  $\text{Ce}^{4+}$  (cerium (IV) oxide). Labels for peaks  $B_0$ ,  $B_1$  and C are provided

platinum crystallites blocking the smaller pores of the support.

### 3.2 X-ray Absorption Near Edge Spectroscopy (XANES)

To directly monitor the reduction of the catalyst in  $\text{H}_2$ , in situ TPR-XANES was employed, as the white line provides information about the density of unoccupied states above the Fermi level. In our previous studies [23, 37], TPR-XANES investigations of a series of Pt/ceria catalysts having different Pt loadings and Ca doped Pt/ceria catalysts definitively identified that once Pt oxide reduction occurs, reduction of the ceria surface shell follows. The latter step was found to involve conversion of surface O to Type II bridging OH groups [17], with a corresponding change in oxidation state of the associated Ce atoms in the surface shell from  $\text{Ce}^{4+}$  to  $\text{Ce}^{3+}$ . Moreover, a significant metal-support interaction was identified, in which systematic increases in Pt loading led to corresponding decreases in reduction temperature of the surface shell. For example, with a very high loading of 5%Pt, surface shell reduction occurred at just 200°C. When the same amount of platinum loading was introduced to calcium doped ceria supports, the broad peak of surface shell reduction shifted to remarkably lower temperatures (e.g., 200–250°C).

The Ce  $L_{\text{III}}$  edge ( $L_{\text{III}} = 5723 \text{ eV}$ ) was also examined for each catalyst over a series of reduction temperatures in flowing hydrogen. As displayed in Figure 1, the XANES line shapes of  $\text{Ce}^{3+}$  and  $\text{Ce}^{4+}$  oxidation states are very different. Peak C for  $\text{Ce}^{4+}$  has been assigned to absorption

into the  $5d$  level with no occupancy in  $4f$  for either the initial or final state, and, while present in completely oxidized  $\text{CeO}_2$ , it is virtually absent for  $\text{Ce}^{3+}$ . The final state configuration may be written  $\text{Ce} [2p^5 4f^0 5d^1] \text{O} [2p^6]$ . The peak labeled B is split into at least two separate assignments [38, 39]. Peak  $B_1$ , also present in the  $\text{CeO}_2$  sample (i.e.,  $\text{Ce}^{4+}$ ), has been assigned to absorption into the  $4f$  level in the final state. That is, in addition to an electron excited from the Ce  $2p$  shell to the  $5d$  shell, another electron is excited, coming from the valence band (i.e., the O  $2p$  shell) to the Ce  $4f$  shell, leaving a hole in the valence band. For the sake of brevity, the simplest final state configuration associated with  $B_1$  may be written  $\text{Ce} [2p^5 4f^1 5d^1] \text{O} [2p^5]$ . During reduction, peaks  $B_1$  and C decrease and a new peak,  $B_0$ , develops, occurring just below that of  $B_1$ , and associated with absorption into the  $5d$  level, with  $4f$  occupancy in the initial state. Its final state configuration may be written  $\text{Ce} [2p^5 4f^1 5d^1] \text{O} [2p^6]$ . The intensity of  $B_0$  is very high for any  $\text{Ce}^{3+}$  reference, with one example (cerous carbonate) provided in Figure 1. These key features ( $B_0$  for  $\text{Ce}^{3+}$  and both  $B_1$  and C as a fingerprint for  $\text{Ce}^{4+}$ ) were used to gain insight into the degree of reduction of the ceria catalyst component.

TPR-XANES trajectories of 0.5% platinum loaded undoped, La, Ba, Y, Hf, and Zn doped ceria catalysts are presented in Figure 2. The degree of reduction of ceria was quantified by carrying out a linear combination fitting of XANES spectra for treated catalysts with WinXAS [32], with reference compounds for  $\text{Ce}^{3+}$  and  $\text{Ce}^{4+}$  oxidation states, in the range of 5.69 and 5.75 keV. Results of the fitting procedure are shown in Figure 3. TPR begins with ceria presenting the  $\text{Ce}^{4+}$  oxidation state. The two steps of reduction (i.e., surface shell reduction and bulk reduction) of undoped ceria with 0.5% Pt, and surface shell reduction was complete ( $\sim 20\%$  of Ce as  $\text{Ce}^{3+}$ ) between 300 and 350°C as shown in Figure 3. In our previous investigation, [37] TPR-XANES of an undoped pure ceria identified that surface shell reduction was complete ( $\sim 25\%$  of Ce as  $\text{Ce}^{3+}$ ) between 450 and 500°C. Addition of Pt shifted the surface shell reduction but did not significantly impact the extent of ceria reduction or its bulk reduction. Ba, La, Y, Hf and Zn doped ceria samples display a decrease in reduction temperature and a significant increase in the extent of Ce reduction. For the Ba doped sample, the extent of Ce reduction is 25% as  $\text{Ce}^{3+}$  at 300°C, for the La doped sample, the extent of Ce reduction is 30% as  $\text{Ce}^{3+}$  at 300°C, and Zn doped sample it is 35% as the  $\text{Ce}^{3+}$  at 300°C, for Y doped sample it is found to be 40% as the  $\text{Ce}^{3+}$  at 300°C. Whereas for the Hf doped sample, the extent of Ce reduction is 80% as  $\text{Ce}^{3+}$  at 300°C. A similar decrease in the temperature of the surface reduction step was also observed in the case of zirconia [35] and calcium [37] doped ceria catalysts promoted with Pt and this

**Fig. 2** TPR-XANES trajectories of 0.5% platinum loaded undoped and Ba, La, Hf, Y, and Zn doped ceria

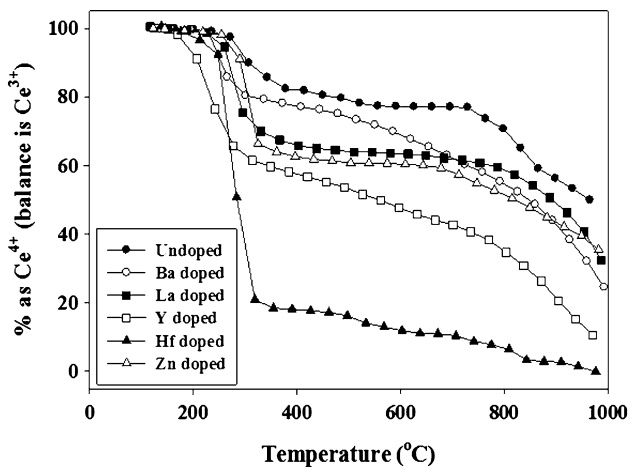
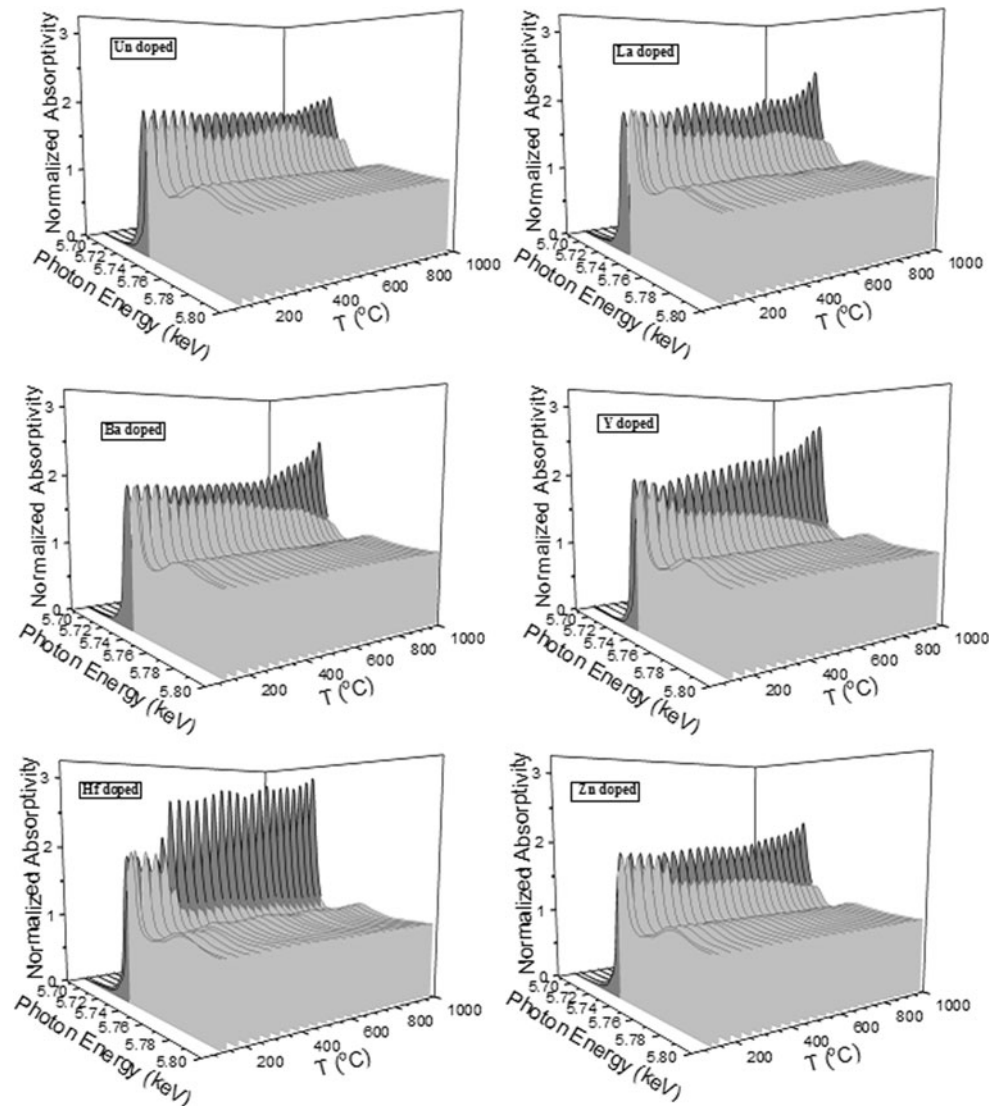


**Fig. 3** Percentage of  $Ce^{4+}$  in the cerium component, balance  $Ce^{3+}$ , along the TPR trajectory of 0.5% platinum loaded undoped and Ba, La, Hf, Y, and Zn doped ceria

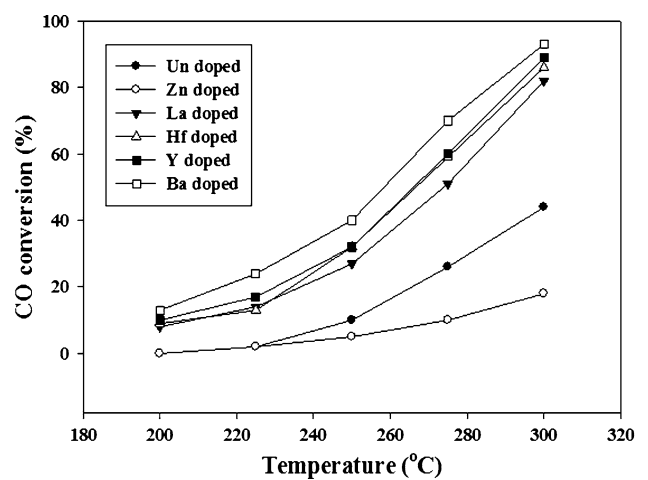
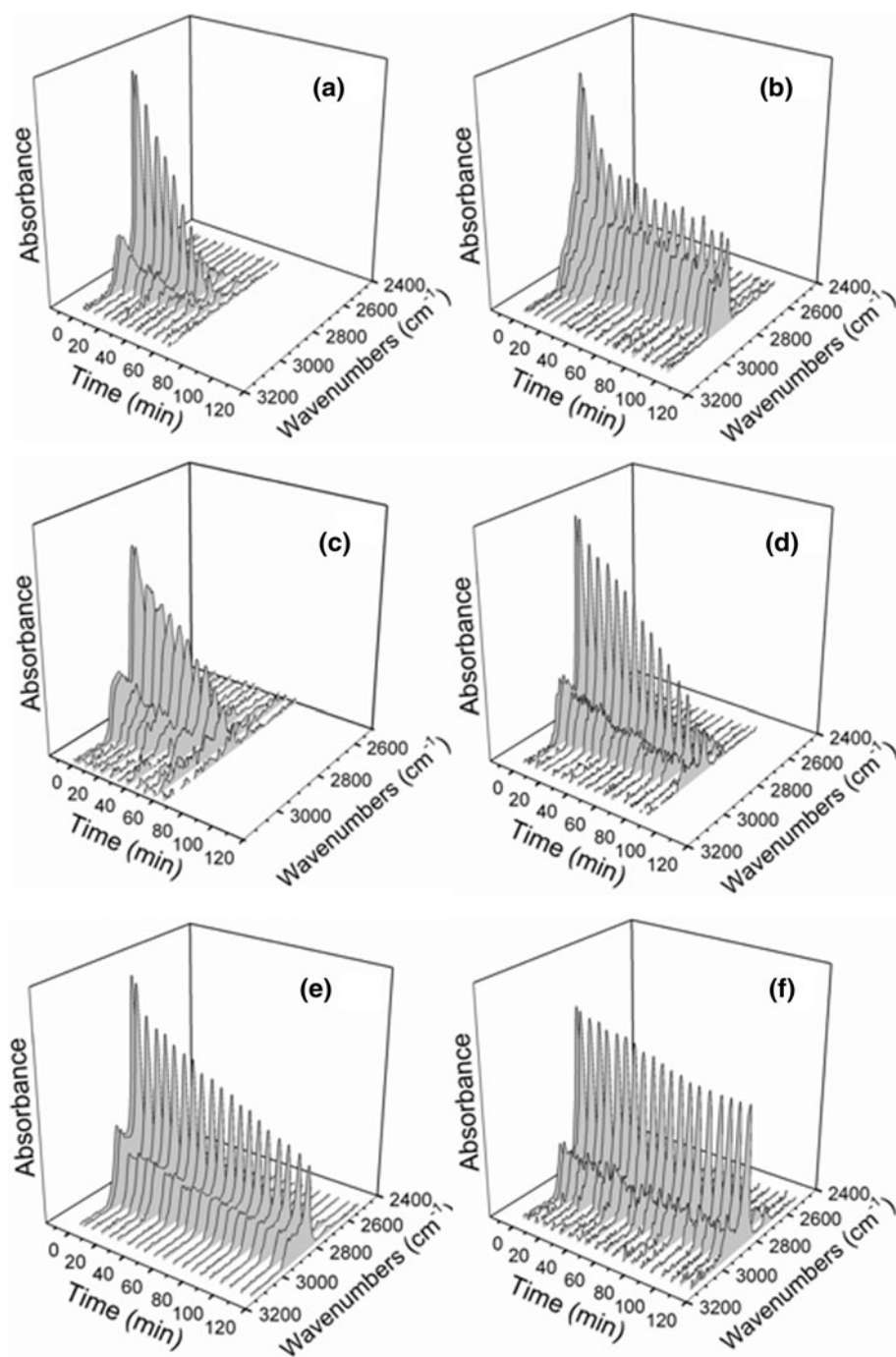


**Fig. 4** Carbon monoxide conversion as a function of temperature for 0.5% platinum loaded undoped and Ba, La, Hf, Y, and Zn doped ceria

**Fig. 5** Transient formate decomposition at 130°C over 0.5% Pt/ceria catalysts doped with **a** Ba **b** Y **c** Hf **d** La **e** undoped and **f** Zn



was taken as evidence for an enhancement in surface O-mobility.

### 3.3 Catalytic Testing Using a Fixed Bed Reactor

Results of catalytic performance tests obtained over the Pt/Ce-Me-O catalysts are presented in Figure 4, where the conversion of CO ( $X_{CO}$ ) is plotted as a function of reaction temperature. The dopants have different effects on catalytic behavior of the modified Pt/CeO<sub>2</sub> catalysts. It is observed

that doping of Pt/ceria with Y, Hf, La and especially Ba, results in a shift of the conversion curves toward lower reaction temperatures, compared to the undoped catalyst. All catalysts were selective to WGS products (CO<sub>2</sub> and H<sub>2</sub>). At 300°C, the CO conversion for the 0.5% Pt/CeO<sub>2</sub> catalyst was 44% while CO conversion increases to 82, 86, 89 and 93% when the reaction was conducted over 0.5% Pt/Ce<sub>0.5</sub>La<sub>0.5</sub>O<sub>1.5</sub>, 0.5% Pt/Ce<sub>0.5</sub>Hf<sub>0.5</sub>O<sub>1.5</sub>, 0.5% Pt/Ce<sub>0.5</sub>Y<sub>0.5</sub>O<sub>1.5</sub>, and 0.5% Pt/Ce<sub>0.5</sub>Ba<sub>0.5</sub>O<sub>1.5</sub> catalysts, respectively. Whereas, for the 0.5% Pt/Ce<sub>0.5</sub>Zn<sub>0.5</sub>O<sub>1.5</sub> catalyst the

CO conversion was found to be 18%, which is lower than the undoped Pt/ceria catalyst. These results are in good agreement with the results of other studies [23–26, 33–37], that the oxide support has a strong influence on the WGS activity. The implication is that Ba, Y, Hf, and La strains the lattice, improving the O-mobility. This in turn improves the mobility of O-bound intermediates which are proposed to form on the support and then migrate and decompose at the Pt–oxide interface. To test the viewpoint further, we turn to results of DRIFTS spectroscopy.

### 3.4 Diffuse Reflectance Fourier Transform Infrared Spectroscopy (DRIFTS)

As described in the experimental section, transient forward formate decomposition tests were carried out at 130°C and with only 3% H<sub>2</sub>O in order to slow down the decomposition so that comparisons could be made (Fig. 5). The band assignments for formate are well known [37]. Here, we are following bands in the formate  $\nu(\text{C-H})$  stretching region as opposed to those in the  $\nu(\text{OCO})$  region, since the latter overlap with the bending mode of H<sub>2</sub>O. The half-lives were found to vary inversely with CO conversion levels, suggesting that the decomposition of an associated intermediate such as formate may indeed be responsible for WGS catalysis. The trend was as follows: Zn-doped (249.0 min) > undoped Pt/ceria (80.4 min) > La-doped (56.2 min) > Hf-doped (37.1 min) > Y-doped (36.0 min) > Ba-doped (24.8 min). However, it should be noted that a bend was observed in the decomposition curve for the Y-doped sample, indicating that a fraction (i.e., in fact, a higher fraction) of the formates decomposed more rapidly. It is unclear at this time why this is the case, but possibilities include: (a) regions of the oxide may have enrichment of one oxide phase, leading to a fraction of less reactive formates; or (b) formates in particular regions of the oxide surface may be less accessible to Pt particles for decomposition. Furthermore, of all the catalysts screened, the Zn-doped catalyst, which displayed enhanced reducibility of ceria, exhibited lower formate decomposition and WGS rates. Again, this may be the result of surface enrichment by Zn oxide, or that the catalysts were not optimized for dopant loading.

## 4 Conclusions

Pt/ceria catalysts doped with specific cations (i.e., Ba, La, Y, Hf and Zn) were characterized by TPR-XANES and transient formate decomposition in order to determine whether dopant addition impacted reducibility (i.e., which in turns governs the temperature at which activation of the surface bridging OH groups takes place) and the mobility

of formate, as O-bound associated species are proposed to be intermediates in the low temperature WGS reaction. TPR-XANES measurements showed that adding dopants to ceria do facilitate catalyst reduction, increasing extents of both surface shell and bulk reduction of ceria, and allowing bridging OH group formation to occur at lower temperature. CO adsorption was used to probe the active bridging OH groups to form formates. DRIFTS measurements of the transient decomposition of formates in steam at low temperature and low H<sub>2</sub>O concentration suggest that formate half-life follows the trend Zn > undoped ceria > La > Hf > Y > Ba, indicating that the formate decomposition rate is enhanced by the addition of most of the dopants tested. Low temperature water–gas shift activity showed good agreement with this trend, with activity following the order: Ba > Y > Hf > La > undoped ceria > Zn. Thus, the results suggest that dopant addition can significantly improve the WGS rate by facilitating catalyst activation and increasing the O-mobility of O-bound associated intermediates (e.g., formates). Moreover, the consequences are that lower amounts of Pt and Ce are required in the formulation to achieve comparable levels of activity.

**Acknowledgments** The work carried out at the CAER was supported in part by funding from the Commonwealth of Kentucky. Argonne’s research was supported in part by the U.S. Department of Energy (DOE), Office of Fossil Energy, National Energy Technology Laboratory (NETL). The use of the Advanced Photon Source was supported by the U.S. Department of Energy, Office of Science, Office of Basic Energy Sciences, under Contract No. DE-AC02-06CH11357. MRCAT operations are supported by the Department of Energy and the MRCAT member institutions.

## References

1. Vielstich W, Lamm A, Gasteiger HA (2003) Handbook of fuel cells: fundamentals, technology, and applications. Wiley, Chichester
2. Song C (2002) Catal. Today 77:17–49
3. Koci P, Schejbal M, Trdlicka J, Gregor T, Kubicek M, Marek M (2007) Catal. Today 119:64–72
4. Koci P, Plat F, Stepanek J, Bartova S, Marek M, Kubicek M, Schmeisser V, Chatterjee D, Weibel M (2009) Catal. Today 147:S257–S264
5. Mannila P, Salmi T, Haario H, Luoma M, Harkonen M, Sohlo J (1996) Appl. Catal. B 7:179–198
6. Whittington B, Jiang C, Trimm D (1995) Catal. Today 26:41–45
7. Phatak AA, Koryabkina N, Rai S, Ratts JL, Ruettinger W, Farrauto RJ, Blau GE, Delgass WN, Ribeiro FH (2007) Catal. Today 123:224
8. Azzam KG, Babich IV, Seshan K, Lefferts L (2007) J. Catal. 251:163
9. Wang X, Gorte RJ, Wagner JP (2002) J. Catal. 212:225
10. Goguet A, Meunier F, Breen JP, Burch R, Petch MI, Chenciu AF (2004) J. Catal. 226:382
11. Fu Q, Deng W, Saltsburg H, Flytzani-Stephanopoulos M (2005) Appl. Catal. B 56:57
12. Wang X, Gorte RJ (2003) Appl. Catal. A 247:157



13. Kundakovic L, Flytzani-Stephanopoulos M (1998) *Appl. Catal. A* 171:13
14. Qi X, Flytzani-Stephanopoulos M (2004) *Ind. Eng. Chem. Res.* 43:3055
15. Shido T, Iwasawa Y (1993) *J. Catal.* 141:71
16. Shido T, Iwasawa Y (1992) *J. Catal.* 136:493
17. Laachir A, Perrichon V, Badri A, Lamotte J, Catherine E, Lavalley JC, El Fallah J, Hilaire L, Le Normand F, Quemere E, Sauvion GN, Touret O (1991) *J. Chem. Soc. Faraday Trans.* 87:1601
18. Lamotte J, Lavalley JC, Druet E, Freund E (1983) *J. Chem. Soc. Faraday Trans.* 79:2219
19. Holmgren A, Andersson B, Duprez D (1999) *Appl. Catal. B* 22:215
20. Jacobs G, Patterson P, Williams L, Graham U, Sparks DE, Davis BH (2004) *Appl. Catal. A: Gen.* 269:63
21. Jacobs G, Chenu E, Patterson P, Williams L, Sparks D, Davis BH (2004) *Appl. Catal.* 258:203
22. Zalc JM, Sokolovskii V, Löffler DG (2002) *J. Catal.* 206:169
23. Jacobs G, Graham UM, Chenu E, Patterson PM, Dozier A, Davis BH (2005) *J. Catal.* 229:499–512
24. Jacobs G, Davis BH (2007) *Appl. Catal. A: Gen.* 333:192–201
25. Jacobs G, Ricote S, Patterson PM, Graham UM, Dozier A, Khalid S, Rhodus E, Davis BH (2005) *Appl. Catal. A: Gen.* 292:229–243
26. Duprez D (2006) *Catal. Today* 112:17–22
27. Burch R (2010) *Platinum Met. Rev.* 54:137–146
28. Jacobs G, Davis BH (2010) *Int. J. Hydrogen Energy* 35: 3522–3536
29. Andreeva D, Kantcheva M, Ivanov I, Ilieva L, Sobczak JW, Lisowski W (2010) *Catal. Today* 158:69–77
30. Yamamoto T, Suzuki A, Nagai Y, Tanabe T, Dong F, Inada Y, Nomura M, Tada M, Iwasawa Y (2007) *Angew Chem Int Ed* 46:9253
31. Jacoby M (2001) *Chem Eng News* 79(32):33–38
32. T. Ressler, WinXAS 97, Version 1.0, 1997
33. Jacobs G, Williams L, Graham U, Sparks D, Thomas G, Davis BH (2003) *Appl. Catal. A: Gen.* 252:107–118
34. Jacobs G, Ricote S, Graham UM, Patterson PM, Davis BH (2005) *Catal. Today* 106:259–264
35. Ricote S, Jacobs G, Milling M, Ji Y, Patterson PM, Davis BH (2006) *Appl. Catal. A: Gen.* 303:35–47
36. Jacobs G, Patterson PM, Calico-Williams L, Chenu E, Sparks DE, Thomas GA, Davis BH (2004) *Appl. Catal. A: Gen.* 262: 177–187
37. Linganiso LZ, Jacobs G, Azzam KG, Graham UM, Davis BH, Cronauer DC, Kropf AJ, Marshall CL (2011) *Appl. Catal. A: Gen.* 394:105–116
38. Overbury S, Huntly D, Mullins D, Glavee G (1998) *Catal Lett* 51:133
39. El Fallah J, Boujani S, Dexpert H, Kiennemann A, Majerus J, Touret O, Villain F, Le Normand F (1994) *J Phys Chem* 98:5522